GOCE STATISTICAL RE-ENTRY PREDICTIONS

J. Geul, E. Mooij, and R. Noomen

Astrodynamics and Space Missions, Delft University of Technology, Kluyverweg 1, 2629 HS Delft, The Netherlands, Email: {j.geul, e.mooij, r.noomen}@tudelft.nl

ABSTRACT

Satellite re-entry predictions are used to determine the time and location of impacts of decaying objects. Large uncertainties result from unknowns in the initial state and environment models. The complex evolution of the attitude further complicates these predictions, especially for slender bodies. Typically, predictions only propagate a point-mass and assume a static error window. Full six degrees-of-freedom (6DOF) statistical re-entry predictions of ESA's Gravity field and steady-state Ocean Circulation Explorer (GOCE) are proposed. Improved error models for the initial state and atmospheric density are introduced. The uncertainty parameters are estimated using Global Positioning System orbit solutions. The predictions are compared against Tracking and Impact Predictions (TIPs) and predictions by the ESA/ESOC Space Debris Office. The 6DOF predictions are consistently closer to the true decay epoch for several starting epochs, while providing narrower windows than TIPs.

Key words: Space Debris; Re-entry Predictions; Error Propagation; Rigid-Body Dynamics.

1. INTRODUCTION

Re-entry predictions are important for determining the impact locations and times of decaying objects. For large spacecraft, with high-temperature resistant components, fragments often survive re-entry and impact Earth. Re-entry predictions can be distinguished by their forecasting period into long- to medium-term, short-term, and break-up and survival predictions. For each type the tools, underlying methods, and analyses are distinct [1].

Short-term predictions range from several days to hours prior to re-entry and focus on predicting the final decay epoch, corresponding to around $80\,\mathrm{km}$ altitude, when break up commonly occurs. The associated uncertainty is often also reported, and is roughly 40% of the remaining orbital lifetime. About 100 Tracking and Impact Predictions (TIPs) are released each year by the Joint Space Operations Center (JSpOC) [1]. Similar predictions are regularly performed by other agencies, institutes, and corporations [2, 3, 4, 5].

In these predictions, the object is modelled as point-mass under the influence of aerodynamic drag acceleration alone [1]. The drag coefficient is known to be dependent on the flight environment and rotational state [6, 7]. Changes with respect to the environment are either not included [2, 4] or through simplified analytic relations [3]. Changes in attitude are even more difficult to accurately model. Especially slender bodies can have multiple stable and tumbling modes, resulting in different drag (and lift) scenarios [8].

All these effects can be accurately modelled with full six degrees-of-freedom (6DOF) simulations, improving the fidelity of the simulations and reducing the number of assumptions on the evolution of the satellite's attitude. 6DOF simulations are already employed in spacecraft-oriented break-up and survival analyses, such as Spacecraft Atmospheric Re-Entry and Aerothermal Breakup (SCARAB) tool by the European Space Agency (ESA) [9], and dispersion analyses of planetary entry vehicles [10]. 6DOF simulations have been previously applied to re-entry predictions of Delta-K rocket bodies [8].

The modelling and quantification of the uncertainties present in the state and models, and subsequent propagation of these uncertainties, can further improve the accuracy of predictions. Most tools assume a static symmetric uncertainty of $\pm 20\%$ of the orbital lifetime on the predicted decay epoch [3, 11]. However, the true boundaries and asymmetry are very sensitive to the atmospheric density and the initial (rotational) state [8], which can vary significantly per re-entry. Statistical methods provide more accurate windows and insight into the shape of the distribution [8, 11].

The paper focuses on improving re-entry predictions of ESA's Gravity field and steady-state Ocean Circulation Explorer (GOCE) satellite, which re-entered on 11 November, 2013 [2]. GOCE's re-entry took significantly longer than initially predicted, due to its aerodynamic shape and controlled attitude, and much lower atmo-

[1] `https://www.space-track.org/#/decay`, accessed: April, 7, 2017

[2] `http://www.esa.int/Our_Activities/Observing_the_Earth/GOCE/Facts_and_figures`, accessed: April, 7, 2017

spheric densities than predicted. The re-entry of GOCE was previously studied by the ESA/ESOC Space Debris Office (SDO) [12] and the Japan Aerospace Exploration Agency (JAXA) [5].

For the re-entry of GOCE, SDO simulated a transition from controlled to uncontrolled motion, by changing the drag coefficient after the attitude controller was assumed to be saturated, effectively using two values for the drag coefficient. For controlled and stable motion the drag coefficient was estimated from GPS and ground station tracking data, while the drag coefficient for uncontrolled motion was obtained as the mean value from 6DOF simulations using SCARAB [12]. The latter drag coefficient was held constant, so is not clear whether the systematic errors in the atmospheric density at the time of re-entry and the dependency on the flight regime were properly accounted for. The atmosphere models are generally not unbiased for the lower regions [13, 14], and especially not during the GOCE re-entry period (see Sec. 3.2).

This paper performs statistical re-entry predictions of GOCE using the 6DOF re-entry simulator as described in [8]. The simulator is extended by modelling GOCE's attitude controller. Further improvements are made to uncertainty models and estimation techniques for the initial translational state and atmospheric density. The parameters are derived from Global Positioning System (GPS) orbit solutions. Finally, the predictions are compared against TIPs and SDO predictions.

The paper is structured as follows. First, the trajectory simulator, including propagation, spacecraft, and environment models, is detailed in Sec. 2. The error propagation and the process of uncertainty modelling and estimation for both GPS- and TLE-derived states is presented in Sec. 3. In Sec. 4, the re-entry predictions are presented, compared, and discussed. Lastly, the conclusions are given in Sec. 5.

2. TRAJECTORY SIMULATION

The explanation of the complete re-entry-prediction simulator is split up in the (deterministic) propagation of a single trajectory (this section), and the modelling, estimation, and propagation of errors (Sec. 3).

GOCE is has a slender aerodynamic shape, which is modelled as a rigid body with attitude control. The drag coefficient for $\alpha = \beta = 0^\circ$ is 3.15, compared to $C_D = 13.24$ for $\alpha = 90^\circ$. For a constantly tumbling motion around the pitch axis the effective mean drag coefficient would be 9.41, almost three times higher than in a stable configuration. Not accounting for the controlled attitude would result in predictions that significantly underestimate the re-entry epoch.

2.1. Propagation

The re-entry simulator consists of a 6DOF trajectory propagator. The complete state is represented by 13 state variables: position and velocity in inertial Cartesian coordinates, attitude quaternion, and the rotational rate in the body-frame. The equations of motion are integrated using a Runge-Kutta-Fehlberg 4(5) variable step-size integrator. The tolerance is set to $\epsilon_{rel} = \epsilon_{abs} = 1 \times 10^{-8}$. The step-size is allowed to vary between a minimum and maximum value of 1×10^{-4} and 1×10^{3} s, respectively. The EGM2008 gravity field model is used up to order and degree 5 [3]. These settings were determined to provide a good trade-off between accuracy and computational efficiency. The atmospheric density is modelled using the NRLMSISE-00 model [14]. The aerodynamic model is explained in further detail below.

2.2. Aerodynamic Model

GOCE is modelled as a combination of 44 flat panels. The mass, centre of mass, and inertia properties of GOCE are provided by ESA for the entire mission duration [4]. For the period after October 28, 2013 the values are:

$$\mathbf{x}_{com} = [2.536,\ 0.004,\ 0.001]\,\mathrm{m} \quad (1)$$

$$m = 1002.152\,\mathrm{kg} \quad (2)$$

$$\mathbf{I} = \begin{pmatrix} 173.0 & 20.2 & -1.7 \\ 20.2 & 2750.5 & -1.1 \\ -1.7 & -1.1 & 2723.2 \end{pmatrix} \mathrm{kg\,m^2} \quad (3)$$

where $\mathbf{x}_{com}$ is the position of the center of mass and $\mathbf{I}$ the inertia tensor with respect to the body-fixed reference frame.

Three seperate flow regimes are considered, namely the free-molecular, transitional, and hypersonic continuum regime. Aerodynamic coefficients are derived for the free-molecular and continuum flow. Shadowing is not taken into account, as its effects are considered negligible for the GOCE panel model. Coefficients for the transitional regime are found using the following bridging function [15]:

$$C_X = F(Kn)(C_{X_{FM}} - C_{X_{cont}}) + C_{X_{cont}} \quad (4)$$

$$F(Kn) = \sin^2\left(\pi \frac{3 + \log_{10} Kn}{8}\right) \quad (5)$$

[3] http://earth-info.nga.mil/GandG/wgs84/gravitymod/egm2008/egm08_wgs84.html, retrieved: March 22, 2017.

[4] https://earth.esa.int/web/guest/-/goce-mass-property-file-8276, retrieved: March 22, 2017.

where $F(Kn)$ is the bridging function, and has a value of 0 at $Kn = 0.001$, 1 at $Kn = 10$, and in between zero and one for $Kn \in (0.001,\ 10)$. The bridging parameters used were derived for the Shuttle, but are also in line with other (blunt) bodies [16].

2.3. Controller Model

GOCE was equipped with magnetorquers to stabilise its attitude. These torquers continued to function throughout the re-entry. For a slender body like GOCE, this has significant impact on the re-entry predictions.

A linear state-feedback controller is implemented to simulate the torque control of GOCE [17]. A control frequency of 10 Hz is chosen. The values of the input and output weighting matrices $\mathbf{Q}$ and $\mathbf{R}$ were obtained from maximum control torques observed during normal operational modes for GOCE and drag-free mode specifications [18]. The gains are solved using optimal control theory. Tab. 1 list the gains of the X, Y, and Z control torques with respect to the aerodynamic angles α, β, and $sigma$, and attitude rates p, q, and r. The gains were solved along a reference trajectory and found to remain constant for altitudes $>60\,\mathrm{km}$.

3. ERROR PROPAGATION

Error propagation is central to performing statistical re-entry predictions. Error propagation, much like regular propagation, solves an initial-value problem, represented by the non-linear transformation of an initial uncertainty under the influence of a stochastic environment over time.

For re-entry predictions the uncertainty in atmospheric density outweighs all other model contributions [19], it is therefore the only environment-model uncertainty considered.

The final decay-time distribution is the uncertainty of main interest. The uncertainty is propagated to obtain a final uncertainty using a Monte-Carlo (MC) simulator. The uncertainties are modelled as a deviation on top of the nominal state. The probability density function (PDF) of the decay-time is estimated using kernel-density estimation (KDE). For each simulation 1000 samples are used, which was determined to provide sufficient convergence of the final distribution.

3.1. Initial State Uncertainty

The translational uncertainty is modelled as a six-dimensional multi-variate normal (MVN) distribution. The translation uncertainty is expressed in the orbital frame as the radial, along-track, and cross-track position and velocity, in which the errors behave quasi-normal.

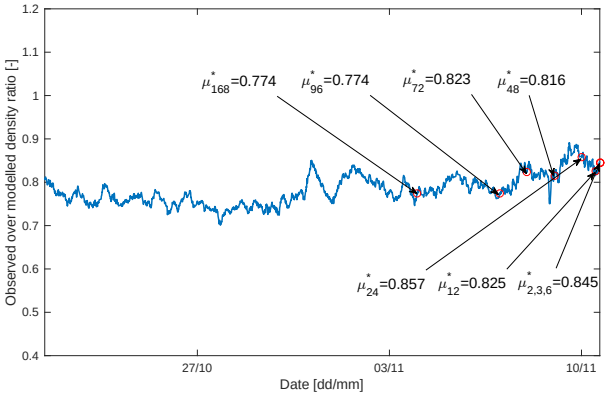

Figure 1. Estimated mean density error $\mu^\star$ for GPS-based density estimates.

Tabs. 2 and 3 give the estimates of the initial translational uncertainty obtained from the orbit determination residuals of November 9, 2013.

Uncertainty in the initial rotational state is assumed to be distributed uniformly within the maximum values for the drag-free mode [18]. The values are given in Tab. 4.

3.2. Atmospheric Density Uncertainty

The atmospheric density has a log-normal uncertainty. The mean and variance mainly depend on the altitude and space-weather conditions. The uncertainty for the $120-200\,\mathrm{km}$ altitude range was derived in [8] and found to be $\mu^\star = 0.98$ and $\sigma^\star = 1.13$. The uncertainty for the $200-400\,\mathrm{km}$ altitude range is $\mu^\star = 0.93$ and $\sigma^\star = 1.17$ [14]. Note that the mean here is an average mean and can vary significantly depending on space-weather conditions. In [13] several atmospheric models are compared for altitudes ranging from 150-240 km. It is found that the mean is typically given within $\pm 10\,\%$ and a standard deviation around $15\,\%$.

The parameters $\mu^\star$ and $\sigma^\star$ can be estimated in several ways. In [8], values from literature were used, which presents a conservative approach. Estimating the parameters for a specific re-entry will provide more narrow and tailored uncertainty distributions. For this, however, additional data is required.

GPS-derived non-gravitational accelerations (as obtained by [20]) are used to estimate uncertainty parameters. The ratio of observed and modelled accelerations is computed. Fig. 1 shows the 10-minute averaged density ratios. The estimate of $\sigma^\star$ is obtained by subtracting the 10-minute averaged signal from the 10 Hz signal. The value for the entire analysis period is used and estimated to be 1.082.

For the estimates of $\mu^\star$ the average over one orbital revolution is taken at several epochs prior to re-entry: 168, 96, 72, 48, 24, 12, 6, 3, and 2 hours. These values are

Table 1. Gains for the LQR controller.

	α	β	σ	p	q	r
K_X	0	3.92×10^{-3}	-1.60 $\times 10^{-2}$	1.00×10^{1}	0	0
K_Y	2.67×10^{-2}	0	0	0	1.33×10^{2}	0
K_Z	0	-3.17×10^{-1}	3.92×10^{-2}	0	0	1.00×10^{2}

Table 2. Initial standard deviation of errors of GPS-derived state.

σ_{r_R} cm	σ_{r_S} cm	σ_{r_W} cm	σ_{v_R} $\mathrm{mm\,s^{-1}}$	σ_{v_S} $\mathrm{mm\,s^{-1}}$	σ_{v_W} $\mathrm{mm\,s^{-1}}$
1.03	12.7	1.31	0.15	0.009	0.016

Table 3. Correlation matrix for initial state obtained through POD from GPS.

	r_R	r_S	r_W	v_R	v_S	v_W
r_R	1.00	0.80	-0.03	-0.80	-0.93	-0.06
r_S	0.80	1.00	-0.00	-1.00	-0.54	-0.05
r_W	-0.03	-0.00	1.00	0.00	0.04	0.02
v_R	-0.80	-1.00	0.00	1.00	0.55	0.05
v_S	-0.93	-0.54	0.04	0.55	1.00	0.06
v_W	-0.06	-0.05	0.02	0.05	0.06	1.00

also indicated in the figure.

4. RESULTS

Apart from the final decay message, seven TIP messages were released for GOCE at various epochs prior to re-entry. SDO has similarly performed several predictions prior to re-entry. SDO predictions started on October 23, 2013, with the assumption that the attitude controller would fail for a $20\,\mathrm{mN}$ drag threshold, resulting in tumbling motion. These early predictions placed the re-entry at around November 6. From November 1, 2013, the threshold was raised to $50\,\mathrm{mN}$. Later, the saturation of the attitude controllers was expected to occur late into the re-entry [12]. Only these last predictions are used for the comparison.

For the 6DOF predictions, it is chosen to start the re-entry predictions at common TIP moments prior to the true re-entry epoch; these are 2h, 3h, 6h, 12h, 1d, 2d, 3d, 4d, and 7d prior to the true decay epoch.

Fig. 2 shows the results for this analysis. The horizontal axis corresponds to date of prediction, and the vertical axis to the prediction error as a percentage of time to decay (TTD). For each prediction the confidence interval (CI) and median is indicated. As a general trend the relative prediction window (as a percentage of the TTD) remains roughly constant. The 6DOF, TIP, and SDO intervals are on average 46%, 65%, and 43% wide, respectively. All are thus wider than the 40% rule of thumb [21, 22].

Table 4. Bounds on uniform rotational uncertainty [18].

		Roll	Pitch	Yaw
Attitude	rad	± 0.15	± 0.06	± 0.15
Rates	$\mathrm{mrad\,s^{-1}}$	± 0.20	± 0.03	± 0.20

The CIs of the TIPs were 41% wider than for 6DOF. The smaller widths for 6DOF can be attributed to the attitude controller, which reduces the rotational uncertainty, leaving only the atmospheric uncertainty as the main driver of the width. A true comparison with the TIP window, of course, depends on the probability of the CI, for which only empirical values are available from old sources [21]. As the TIP window for GOCE is significantly wider than the 40% earlier mentioned, it could be the TIP window and process have changed.

For all predictions the median of the 6DOF is found to be closer to the true re-entry epoch, compared to the window mid-points of the closest TIP and SDO's medians. The 6DOF distributions are slightly asymmetric, where the median is on average located at 7.3% (in terms of the total distribution width) from the midpoint towards the lower bound. This is characteristic for decay-time distributions, where long re-entries are more likely than short re-entries.

Except for the final three predictions (6, 3, and 2h), respectively, the median overshoots the true decay epoch. A maximum of 10% (about 5 hours) is observed for the prediction made at 48 hours prior. The median of the SDO predictions is in all cases earlier (13% on average) than the true re-entry epoch. The difference grows for the last 2 prediction epochs, hinting perhaps at an issue with the later stages of the prediction. Two possible explanations were already discussed: not taking the low densities into account in the SCARAB-derived drag coefficient and/or keeping the drag-coefficient invariant of the flight environment.

5. CONCLUSIONS

The decay-time distribution accuracy for GOCE is dominated primarily by systematic errors in atmospheric density and attitude control, while its precision is dominated by the atmospheric uncertainty. This is followed by the initial translational uncertainty.

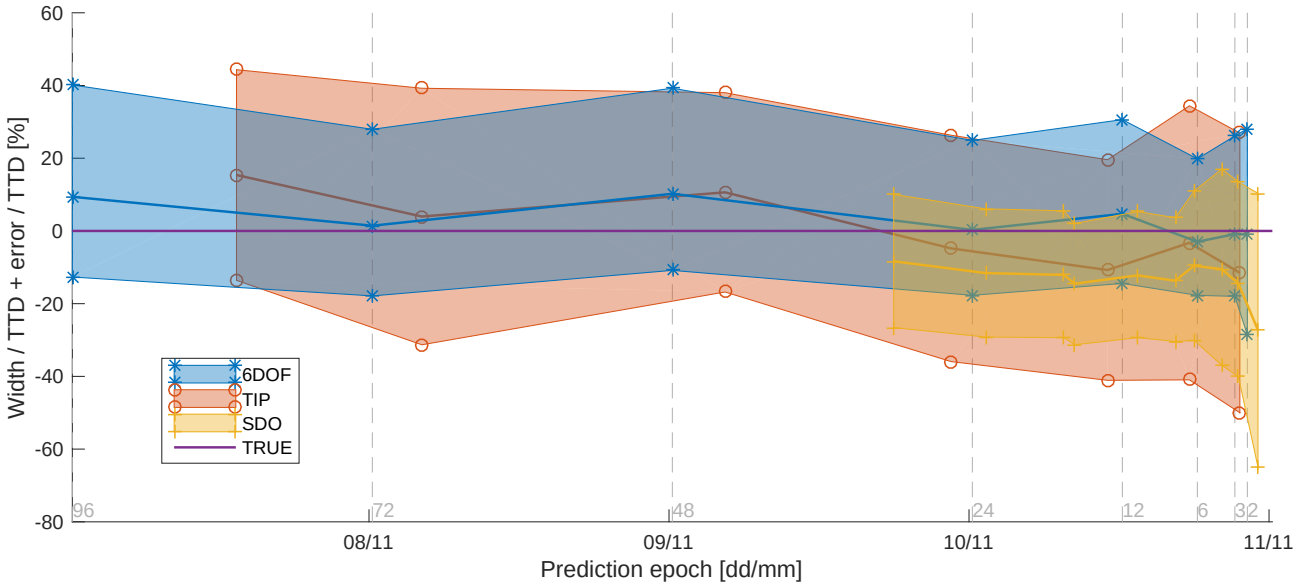

Figure 2. Comparison of 6DOF with TIPs and SDO re-entry predictions for several prediction epochs.

By analysing the density-modelling error from GPS-derived non-gravitational accelerations, a better estimate of the density uncertainty could be obtained. The attitude control is found to prolong the re-entry significantly. By modelling the attitude control and motion in a 6DOF simulator, it is not necessary to assume a constant drag coefficient and introduce any discontinuities to this value.

The median of the 6DOF re-entry predictions was found consistently closer to the true decay epoch than neighbouring TIPs and predictions by SDO. Moreover, the TIP window was found to be on average 41% wider than for 6DOF. The 6DOF and SDO predictions are found to be of comparable relative width. The SDO predictions already employed 6DOF techniques to determine the final drag coefficients for the 3DOF propagation. Two potential implementation issues with this approach were identified.

It is recommended to perform full 6DOF re-entry predictions for objects for which aerodynamic models are available or can be easily constructed. For instance, for rocket bodies a single model can be used for many re-entry predictions.

ACKNOWLEDGEMENT

This work is supported by the European Office for Aerospace Research and Development (EOARD), grant FA9550-14-1-0344.

The work described in this paper was partly carried out in the framework of the European Space Agency (ESA) study on benchmarking reentry prediction uncertainties under Contract no. 400011517/15/F/MOS. ESA is also acknowledged for kindly providing all the required GOCE observation data and supporting information.

REFERENCES

1. Klinkrad, H., Fritsche, B., and Koppenwallner, G., "Re-Entry Prediction and On-Ground Risk Estimation," *Space Debris - Models and Risk Analysis*, edited by H. Klinkrad, chap. 9, Springer Verlag, Berlin.
2. Strizzi, J. D., *An Improved Algorithm for Satellite Orbit Decay and Re-Entry Predictions*, MSc thesis, Massachusetts Institute of Technology, 1993.
3. Klinkrad, H., "Methods and Procedures ofr Re-Entry Predictions at ESA," *European Conference on Space Debris*, Vol. 6, 2013.
4. Anselmo, L. and Pardini, C., "Satellite reentry predictions for the Italian civil protection authorities," *Acta Astronautica*, Vol. 87, 2013, pp. 163–181, doi: 10.1016/j.actaastro.2013.02.004.
5. Ikeda, S., Tajima, T., Abe, J., and Matsuda, I., "Improved Re-Entry Prediction Method," *SpaceOps Conference*, No. AIAA 2014-1836, 2014.
6. Crowther, R., "Re-entry Aerodynamics Derived from Space Debris Trajectory Analysis," *Planetary and Space Science*, Vol. 40, No. 5, 1992, pp. 641–646.
7. Bowman, B. R. and Moe, K., "Drag coefficient variability at 100-300 km from the orbit decay analyses of rocket bodies," *AIAA/AAS Astrodynamics Specialist Conference*, , No. AAS 05-256, 2005.
8. Ronse, A. and Mooij, E., "Statistical Impact Prediction of Decaying Objects," *Journal of Spacecraft and Rockets*, Vol. 51, No. 6, 2014, pp. 1797–1810.
9. Koppenwallner, G., Fritsche, B., Lips, T., and Klinkrad, H., "SCARAB - A Multi-Disciplinary Code for Destruction Analysis of Spacecraft During Re-Entry," *European Symposium on Aerothermodynamics for Space Vehicles*, 2005.

10. Desai, P. N., Schoenenberger, M., and Cheatwood, F. M., "Mars Exploration Rover Six-Degree-of-Freedom," *Journal of Spacecraft and Rockets*, Vol. 43, No. 5, 2006, pp. 1019–1025, doi: 10.2514/1.6008.

11. Neuenfeldt, B., *A survey of uncontrolled satellite reentry and impact prediction*, MSc thesis, Naval Postgraduate School, 1993.

12. Virgili, B. B., Flohrer, T., Lemmens, S., and Krag, H., "GOCE Re-entry Campaign," *5th International GOCE User Workshop*, No. ESA SP-728, 2014.

13. Marcos, F. A., "Accuracy of atmospheric drag models at low satellite altitudes," *Advances in Space Research*, Vol. 10, No. 3-4, 1990, pp. 417–422, doi: 10.1016/0273-1177(90)90381-9.

14. Picone, J. M., Hedin, A. E., Drob, D. P., and Aikin, A. C., "NRLMSISE-00 Empirical Model of the Atmosphere: Statistical Comparisons and Scientific Issues," *Journal of Geophysical Research*, Vol. 107, No. A12, 2002, pp. 1468–1483, doi: 10.1029/2002JA009430.

15. Blanchard, R. C. and Buck, G. M., "Rarefied-flow Aerodynamics and Thermosphere Structure from Shuttle Flight Measurements," *Journal of Spacecraft and Rockets*, Vol. 23, No. 1, 1986, pp. 18–24.

16. Wilmoth, R. G., Blanchard, R. C., and Moss, J. N., "Rarefied Transitional Bridging of Blunt Body Aerodynamics," *Symposium on Rarefied Gas Dynamics*, 1998.

17. Mooij, E., *The Motion of a Vehicle in a Planetary Atmosphere*, Series 08: Astrodynamics and Satellite Systems 01, Delft University Press, 1997.

18. Sechi, G., André, G., Andreis, D., and Saponara, M., "Magnetic attitude control of the GOCE satellite," *Guidance, navigation and control systems*, , No. 606, 2006.

19. Klinkrad, H., "On the Use of Atmosphere Models in Re-Entry Predictions," *Environment Modelling for Space-based Applications*, No. SP-392, 1996, pp. 287–298.

20. Visser, P. N. A. M. and van den IJssel, J. A. A., "Orbit determination and estimation of non-gravitational accelerations for the GOCE reentry phase," *Advances in Space Research*, Vol. 58, No. 9, 2016, pp. 1840–1853, doi: 10.1016/j.asr.2016.07.013.

21. Lefebvre, S., *An Analysis of Tracking and Impact Predictions*, MSc thesis, Air Force Institute of Technology, 1991, No. AFIT/GSO/ENG/91D-11.

22. Kronebusch, R. M., "USAF's Role in Surveillance," *The Space Congress*, No. 16, 1979.